LECTURE NOTES IN COMPUTATIONAL SCIENCE AND ENGINEERING 82

Björn Engquist · Olof Runborg
Yen-Hsi R. Tsai *Editors*

Numerical Analysis of Multiscale Computations

Springer

Preface

The recent rapid progress in multiscale computations has been facilitated by modern computer processing capability and encouraged by the urgent need to accurately model multiscale processes in many applications. For further progress, a better understanding of numerical multiscale computations is necessary. This understanding must be based on both theoretical analysis of the algorithms and on specific features of the different applications.

We are pleased to present 16 papers in these proceedings of the workshop on Numerical Analysis and Multiscale Computations at the Banff International Research Station for Mathematical Innovation and Discovery, December 6-11, 2009. The papers represent the majority of the presentations and discussions that took place at the workshop. A goal of the workshop was to bring together researchers in numerical analysis and applied mathematics with those focusing on different applications of computational science. Another goal was to summarize recent achievements and to explore research directions for the future. We feel that this proceeding lives up to that spirit with studies of different mathematical and numerical topics, such as fast multipole methods, homogenization, Monte Carlo techniques, oscillatory solutions to dynamical systems, stochastic differential equations as well as applications in dielectric permittivity of crystals, lattice systems, molecular dynamics, option pricing in finance and wave propagation.

Austin and Stockholm,
April 2011

Björn Engquist
Olof Runborg
Yen-Hsi Richard Tsai

Acknowledgements

Use the template *acknow.tex* together with the Springer document class SVMono (monograph-type books) or SVMult (edited books) if you prefer to set your acknowledgement section as a separate chapter instead of including it as last part of your preface.

Contents

27. C. Ortner. The role of the patch test in 2D atomistic-to-continuum coupling methods. arXiv:1101.5256, 2011.
28. C. Ortner and E. Süli. Analysis of a quasicontinuum method in one dimension. *M2AN Math. Model. Numer. Anal.*, 42(1):57–91, 2008.
29. Y. Saad. *Iterative Methods for Sparse Linear Systems*, volume 2. Society for Industrial and Applied Mathematics (SIAM), 2003.
30. A. V. Shapeev. Consistent energy-based atomistic/continuum coupling for two-body potential: 1D and 2D case. arXiv:1010.0512, 2010.
31. V. B. Shenoy, R. Miller, E. B. Tadmor, D. Rodney, R. Phillips, and M. Ortiz. An adaptive finite element approach to atomic-scale mechanics–the quasicontinuum method. *J. Mech. Phys. Solids*, 47(3):611–642, 1999.
32. L. E. Shilkrot, R. E. Miller, and W. A. Curtin. Coupled atomistic and discrete dislocation plasticity. *Phys. Rev. Lett.*, 89(2):025501, 2002.
33. T. Shimokawa, J. Mortensen, J. Schiotz, and K. Jacobsen. Matching conditions in the quasicontinuum method: Removal of the error introduced at the interface between the coarse-grained and fully atomistic region. *Phys. Rev. B*, 69(21):214104, 2004.

Analysis of an Averaging Operator for Atomic-to-Continuum Coupling Methods by the Arlequin Approach

Serge Prudhomme, Robin Bouclier, Ludovic Chamoin, Hachmi Ben Dhia, and J. Tinsley Oden

Abstract A new coupling term for blending particle and continuum models with the Arlequin framework is investigated in this work. The coupling term is based on an integral operator defined on the overlap region that matches the continuum and particle solutions in an average sense. The present exposition is essentially the continuation of a previous work (Bauman et al., On the application of the Arlequin method to the coupling of particle and continuum models, *Computational Mechanics*, 42, 511–530, 2008) in which coupling was performed in terms of an H^1-type norm. In that case, it was shown that the solution of the coupled problem was mesh-dependent or, said in another way, that the solution of the continuous coupled problem was not the intended solution. This new formulation is now consistent with the problem of interest and is virtually mesh-independent when considering a particle model consisting of a distribution of heterogeneous bonds. The mathematical properties of the formulation are studied for a one-dimensional model of harmonic springs, with varying stiffness parameters, coupled with a linear elastic bar, whose modulus is determined by classical homogenization. Numerical examples are pre-

S. Prudhomme
Institute for Computational Engineering and Sciences (ICES), The University of Texas at Austin, 1 University Station C0200, Austin, TX 78712, U.S.A., e-mail: serge@ices.utexas.edu

R. Bouclier
Laboratoire de Mécanique et Technologie (LMT-Cachan), Ecole Normale Supérieure de Cachan, 61 Avenue du Président Wilson, 94235 Cachan Cedex, France, e-mail: bouclier@ices.utexas.edu

L. Chamoin
Laboratoire de Mécanique et Technologie (LMT-Cachan), Ecole Normale Supérieure de Cachan, 61 Avenue du Président Wilson, 94235 Cachan Cedex, France, e-mail: chamoin@lmt.ens-cachan.fr

H. Ben Dhia
Laboratoire de Mécanique des Sols, Structures et Matériaux (MSSMat), Ecole Centrale Paris, 1 Grande Voie des Vignes, 92290 Châtenay-Malabry, France, e-mail: hachmi.ben-dhia@ecp.fr

J. T. Oden
Institute for Computational Engineering and Sciences (ICES), The University of Texas at Austin, 1 University Station C0200, Austin, TX 78712, U.S.A., e-mail: oden@ices.utexas.edu

sented for one-dimensional and two-dimensional model problems that illustrate the approximation properties of the new coupling term and the effect of mesh size.

1 Introduction

Development of multiscale methods for the simulation of material responses is an important research area in which one of the objectives is to combine models so as to capture only the relevant scales in the prediction of complex phenomena. The goal in this work is to develop a new multiscale method to predict the static response of materials that can be described by particle models based on harmonic potentials. Multiscale modeling is commonly classified into information passing modeling, in which information computed at small scales is used in large-scale models, such as in the Heterogeneous Multiscale method [20, 21], and concurrent modeling, in which two or more models are concurrently used to capture the various scales inherent in a given physical phenomenon, see e.g. [22, 23]. We are interested here in concurrent modeling for the simulation of problems that involve both a particle model and a continuum model. The major difficulty in this case is to consistently blend the two models so as to provide accurate approximations of the solution to the full particle model, viewed as the base model but often intractable for large simulation domains. Several methods have been proposed over the years, such as the quasi-continuum method [28, 25, 17, 18, 19], the handshake method [14], or the bridging scale approach [29], to name a few. An alternative approach based on the Arlequin framework [8, 9, 11, 12, 13] has recently been proposed in [5, 10, 26]. The Arlequin framework involves an overlap region in which the energies of the two models are combined by a partition of unity and where the two solutions are matched by introducing Lagrange multipliers. The bridging domain method of Belytschko and Xiao [7] is in many ways similar to the Arlequin method and was numerically investigated in [30]. A related methodology has also been proposed in [24, 2, 3] in which forces, rather than energies, are blended together. The method proposed in [5] was further employed to develop an adaptive procedure based on goal-oriented error estimates (see [4, 6, 27]) to control the position of the overlap region so as to deliver estimates of quantities of interest within prescribed tolerances.

Well-posedness of the Arlequin problems for the continuous and finite element formulations was investigated in detail in [5] in the case of a one-dimensional model of harmonic springs, with periodically varying stiffness coefficients, coupled with a linear elastic bar. Couplings of the displacement fields obtained from the particle and continuum models were defined based on an L^2-norm or an H^1-norm. It was then proved that the continuous formulation and corresponding discretization of the continuous formulation, by the finite element method for instance, yield well-posed problems only in the H^1-norm case. However, it was recognized at that time that the solution of the coupled problem was mesh-dependent in the sense that the finite element approximation of the continuum model would lock on the particle solution on the overlap region when elements for the Lagrange multiplier were chosen

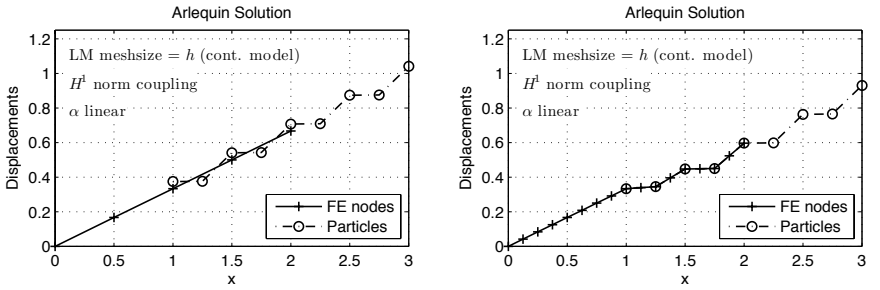

Fig. 1 Solutions of the coupled problem based on the Arlequin framework as proposed in [5] using either a coarse (left) or fine (right) finite element discretization of the continuum model. "Coarse" and "fine" here are defined with respect to the equilibrium length between particles. The coupling term is based on an H^1-type norm. One observes that the continuum solution on the overlap region locks onto the particle solution in the case of the fine mesh for the Lagrange multiplier and FE solution and thus fails to reflect the large-scale behavior of the displacement field.

equal to or smaller than the distance between particles. This issue could be circumscribed by selecting the mesh size for the Lagrange multiplier to be at least larger than the size or a multiple of the size of the representative cell defined to calibrate the parameter(s) of the continuum model, in which case the method would produce satisfactory results. If elements were set too small for the Lagrange multiplier, the continuum solution would fail to reproduce the large-scale behavior of the displacement fields and would pollute the whole solution of the coupled problem. These effects are illustrated in Fig. 1. We propose here a new formulation of the coupling term based on an integral operator that matches the continuum and particle solutions in an average sense. The advantage of this new formulation is that it yields a mesh-independent displacement field. We show in this paper that this new Arlequin formulation yields a well-posed coupled problem and illustrate its efficiency via simple one-dimensional and two-dimensional problems.

The paper is organized as follows: in Sect. 2, we present the particle model and the continuum model and show how the latter is derived from the former by simple homogenization. We introduce the averaging operator and describe the new coupling formulation based on the Arlequin framework in Sect. 3. We show that the coupled problem is well-posed in Sect. 4 and describe the corresponding finite element formulation in Sect. 5. One-dimensional and two-dimensional numerical experiments are presented in Sect. 6 and are followed by conclusions in Sect. 7.

2 Particle and Continuum Model Problems

2.1 Particle Model

We consider here a system of $n+1$ particles assembled in a one-dimensional chain and connected by n covalent bonds modeled in terms of harmonic springs with stiffness $k_i > 0$ and equilibrium length l_i, $i = 1, \ldots, n$. The initial positions of the particles are given by x_i and the system undergoes displacements y_i when subjected to force f applied at x_n (see Fig. 2). We also suppose that the particle on the left end is fixed, i.e. $y_0 = 0$. The potential energy of such a system is given by

$$\mathscr{E}_d(y) = \frac{1}{2}\sum_{i=1}^{n} k_i \left(y_i - y_{i-1}\right)^2 - f y_n. \tag{1}$$

Introducing the vector space $W_0 = \{z \in \mathbb{R}^{n+1} : \, z_0 = 0\}$ of vectors $z = [z_0, z_1, \ldots, z_n]^T$, the equilibrium state $y \in W_0$ of such a system is obtained as a minimizer of the potential energy, i.e.

$$y = \underset{z \in W_0}{\arg\min} \; \mathscr{E}_d(z). \tag{2}$$

In other words, the solution w of above minimization problem is a stationary point of $\mathscr{E}_d(z)$ and satisfies

$$\lim_{\theta \to 0} \frac{1}{\theta} \left(\mathscr{E}_d(y + \theta z) - \mathscr{E}_d(y)\right) = 0, \qquad \forall z \in W_0.$$

It follows that Problem (2) can be recast in variational form as

$$\boxed{\text{Find } y \in W_0 \text{ such that} \quad B(y,z) = F(z), \quad \forall z \in W_0,} \tag{3}$$

where the bilinear form $B(\cdot,\cdot)$ and linear form $F(\cdot)$ are defined as:

$$\begin{cases} B(y,z) = \displaystyle\sum_{i=1}^{n} k_i \left(y_i - y_{i-1}\right)\left(z_i - z_{i-1}\right), \\ F(z) = f z_n. \end{cases} \tag{4}$$

In this paper, we are interested in materials in which the stiffness k_i may vary from one bond to the other. Nevertheless we suppose that the distribution of the bonds are such that the large scales of the material response could be accurately described by a continuum model over representative volume elements (RVE). For instance, in the case of periodic distributions of the bond stiffness k_i, the representative volume element is simply chosen of the same length as one period of the distribution. More complex distributions, for example random, could also be considered (see for example [15]) but the size of the RVE would be unknown a priori. For simplicity in the presentation, we will not present here cases where the energy potentials involve next-nearest neighbors. This has been partially treated in [16].

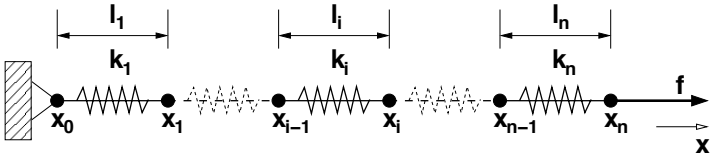

Fig. 2 System of $n+1$ particles connected with n harmonic springs.

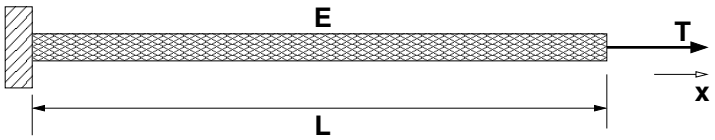

Fig. 3 Elastic bar of length L with modulus of elasticity E and subjected to traction T.

2.2 Continuum Model

If one is interested in large-scale features of the response (in the sense that the scale of those features would be much larger than the representative length-scale of the particle system, e.g. $\max_i(l_i)$), a possible approximation of the particle model can be obtained by employing a linearly elastic continuum model. In this case, the system of springs is replaced by an elastic bar with modulus E and of length L; see Fig. 3. Moreover, the bar is subjected to traction $T = f/A$ at the right end, A being the cross-sectional area of the bar, and is kept fixed at $x = 0$. Displacement in the bar is denoted by the field u. The total energy of the system is then given by

$$\mathscr{E}_c = \int_0^L \frac{A}{2}\sigma(u)\varepsilon(u)\,dx - AT(L)u(L), \tag{5}$$

where $\sigma(u)$ and ε denote the stress and strain in the bar. Here the material is supposed to obey Hooke's law, $\sigma = E\varepsilon$, with E constant. Using $\varepsilon = u'$, we have

$$\mathscr{E}_c = \int_0^L \frac{AE}{2}\left(u'\right)^2\,dx - AT(L)u(L). \tag{6}$$

As with the spring model, the equilibrium state for the continuum model is found by minimizing the energy (6). This minimization yields the following problem:

$$\boxed{\text{Find } u \in V \text{ such that:} \quad \int_0^L Eu'v'dx = T(L)v(L) \qquad \forall v \in V,} \tag{7}$$

where V is the space of trial and test functions, i.e. $V = \{v \in H^1(0,L) :\ v(0) = 0\}$.

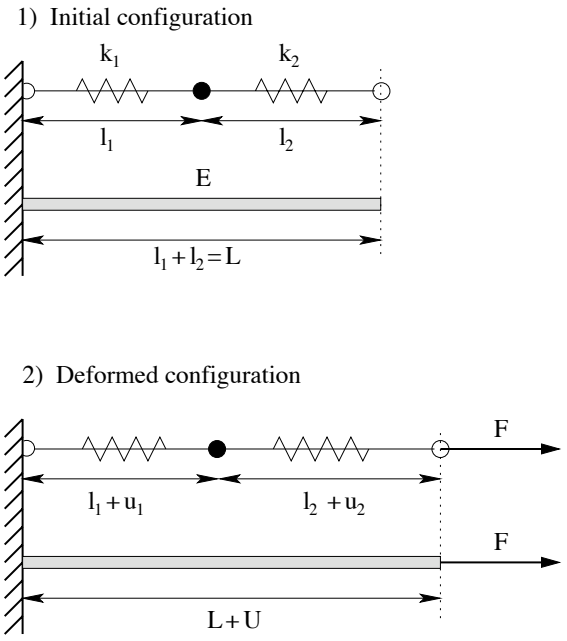

Fig. 4 Homogenization of spring model on a representative cell.

2.3 Calibration of Continuum Model

Starting with the original particle model, it is possible to determine a compatible continuum model by properly calibrating the elastic modulus. Following classical homogenization approaches, the main idea here is to introduce a representative volume element, that, if subjected to a given loading, should provide the same global response at equilibrium, i.e. the same global displacement, when using either the particle or continuum model.

To illustrate the concept, we consider here the simple case of a representative cell consisting of a pair of springs with properties (k_1, l_1) and (k_2, l_2), as shown in Fig. 4. We assume that the system is held fixed on the left-hand side and is subjected to the force F to the right, such that the displacement in the first and second springs are u_1 and u_2, respectively. Suppose now that we can replace the system of two springs by a unique spring with properties (K, L) such that $L = l_1 + l_2$. If subjected to the same loading conditions, we would observe the global displacement $U = u_1 + u_2$. From constitutive laws, we also have the relations:

$$F = KU = k_1 u_1 = k_2 u_2, \tag{8}$$

so that

$$\frac{F}{K} = U = u_1 + u_2 = \frac{F}{k_1} + \frac{F}{k_2}, \tag{9}$$

which implies that:

$$\frac{1}{K} = \frac{1}{k_1} + \frac{1}{k_2}, \qquad \text{i.e.} \quad K = \frac{k_1 k_2}{k_1 + k_2}. \tag{10}$$

Finally, replacing the spring model by linear elasticity, we would obtain the following Young's modulus:

$$\boxed{EA = KL = \frac{k_1 k_2}{k_1 + k_2}(l_1 + l_2),} \tag{11}$$

where A is the cross-sectional area of the equivalent bar. For simplicity, we take A equal to unity.

Remark 1. The above relation can naturally be extended to the case of one RVE made of N springs. In this case, we would have:

$$EA = \left[\sum_{j=1}^{N} 1/k_j\right]^{-1} \sum_{i=1}^{N} l_i. \tag{12}$$

It is then straightforward to show that:

$$EA = \sum_{i=1}^{N} \left[\sum_{j=1}^{N} k_i/k_j\right]^{-1} k_i l_i \geq \min_{1\leq i\leq N}(k_i l_i)\left[\sum_{i=1}^{N} 1/k_i\right]\left[\sum_{j=1}^{N} 1/k_j\right]^{-1} = \min_{1\leq i\leq N}(k_i l_i). \tag{13}$$

In the same manner, we have:

$$EA = \sum_{i=1}^{N} \left[\sum_{j=1}^{N} k_i/k_j\right]^{-1} k_i l_i \leq \max_{1\leq i\leq N}(k_i l_i)\left[\sum_{i=1}^{N} 1/k_i\right]\left[\sum_{j=1}^{N} 1/k_j\right]^{-1} = \max_{1\leq i\leq N}(k_i l_i). \tag{14}$$

In other words, with $A = 1$, one gets:

$$\min_{1\leq i\leq N}(k_i l_i) \leq E \leq \max_{1\leq i\leq N}(k_i l_i), \tag{15}$$

i.e. the value of E is necessarily larger than the minimal value of $k_i l_i$ and smaller than the maximal value of $k_i l_i$.

Remark 2. Starting from the relation $U = u_1 + u_2$, we can write:

$$\frac{U}{L} L = \frac{u_1}{l_1} l_1 + \frac{u_2}{l_2} l_2. \tag{16}$$

We recognize in above equation the strains $\bar{\varepsilon} = U/L$, $\varepsilon_1 = u_1/l_1$, $\varepsilon_2 = u_2/l_2$, which are constant in each spring. Therefore, we can derive the following relationship:

$$\int_{\text{RVE}} \bar{\varepsilon} dx = \int_{\text{RVE}} \varepsilon dx, \tag{17}$$

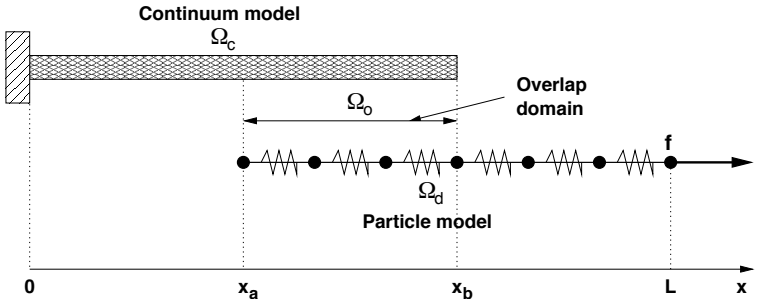

Fig. 5 Arlequin model that replaces the particle model with a combined particle and spring model.

where $\varepsilon = \varepsilon_1$ in the first spring and $\varepsilon = \varepsilon_2$ in the second spring. This relation shows that the averaged strain over the representative volume element is the same whether it is computed from the particle model or the continuum model. This relationship will motivate our new formulation of the coupling method based on an averaging operator.

3 Coupling Method with Averaging Operator

We recall that our objective is to develop a coupling method to blend the particle model with the continuum model in $\Omega = (0,L)$. We assume that the continuum model is selected in region $\Omega_c = (0,x_b)$ while the particle model is chosen in domain $\Omega_d = (x_a,L)$ such that $\Omega = \Omega_c \bigcup \Omega_d$ and $\Omega_o = \Omega_c \bigcap \Omega_d = (x_a,x_b)$, $|\Omega_o| \neq 0$. We will refer to Ω_o as the overlap region. We denote by $|\Omega_c|$, $|\Omega_d|$, and $|\Omega_o|$, the length of domains Ω_c, Ω_d, and Ω_o, respectively. In doing so, the particle model is reduced from $n+1$ to $m+1$ particles, supposedly with $m \ll n$.

Remark 3. We assume in this work that there are m_o+1 particles lying in the overlap region and that there is one particle located at x_a and one at x_b as shown in Fig. 5. The restrictive assumption that is made here is that the overlap region exactly coincides with a given set of complete springs. In other words, the domain Ω_o is not allowed to only cover part of a spring. However, the domain Ω_o can be made of one or several RVE's.

3.1 Energy of the Coupled System

The Arlequin method is an energy-based method in which the energy contributions from two models are blended together via the partition of unity:

$$\alpha_c(x) + \alpha_d(x) = 1, \quad \forall x \in \Omega,$$

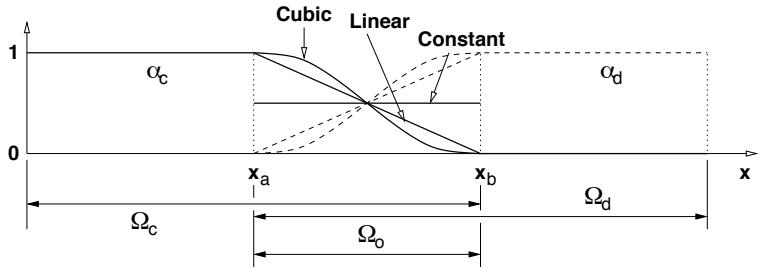

Fig. 6 Plot of different functions used for α_c and α_d.

with

$$\alpha_c(x) = \begin{cases} 1, & \forall x \in \Omega_c \setminus \Omega_o, \\ 0, & \forall x \in \Omega_d \setminus \Omega_o, \end{cases} \qquad \alpha_d(x) = \begin{cases} 0, & \forall x \in \Omega_c \setminus \Omega_o, \\ 1, & \forall x \in \Omega_d \setminus \Omega_o. \end{cases}$$

Weight coefficients with respect to each bond are also introduced as:

$$\alpha_i = \frac{1}{l_i}\int_{x_{i-1}}^{x_i} \alpha_d(x)\, dx = 1 - \frac{1}{l_i}\int_{x_{i-1}}^{x_i} \alpha_c(x)\, dx, \quad i = 1, \ldots, m. \tag{18}$$

In the overlap region Ω_o, the coefficient α_c (and thus α_d) can be chosen in different ways. Some intuitive and apparently attractive candidates are for example, the constant, linear, or cubic functions, as shown in Fig. 6. For example, the cubic function can be explicitly written as:

$$\alpha_c(x) = \left[\frac{x_b - x}{x_b - x_a}\right]^2 \left[1 + 2\frac{(x - x_a)}{(x_b - x_a)}\right], \qquad \forall x \in \Omega_o. \tag{19}$$

The total energy of the molecular system can now be replaced by:

$$\hat{\mathscr{E}}(u, w) = \hat{\mathscr{E}}_c(u) + \hat{\mathscr{E}}_d(w),$$

where

$$\begin{aligned} \hat{\mathscr{E}}_c(u) &= \frac{1}{2}\int_{\Omega_c} \alpha_c(x) E\left(u'\right)^2\, dx, \\ \hat{\mathscr{E}}_d(w) &= \frac{1}{2}\sum_{i=1}^{m} \alpha_i k_i \left(w_i - w_{i-1}\right)^2 - f w_m, \end{aligned} \tag{20}$$

with f, once again, being the external force applied at L, i.e. to the particle indexed by m.

3.2 Averaging Coupling Operator

The objective being to properly couple the two models, the displacements u and w need to be matched with respect to some appropriate measure. In order to be able to compare u and w on Ω_o, the displacement vector w needs first to be converted into a function in $H^1(\Omega_o)$. A possible approach is to introduce an interpolation operator $\Pi_o : \mathbb{R}^{m_o+1} \to H^1(\Omega_o)$, which associates with each displacement vector w (restricted to the particles in Ω_o) the piecewise linear interpolant $\Pi_o w$ on Ω_o. Other interpolation schemes are imaginable, but for the sake of simplicity, we shall only consider the linear interpolant in the present work. We also introduce the restriction operator $\mathrm{R}_o : H^1(\Omega_c) \to H^1(\Omega_o)$ that restricts continuum displacements u to Ω_o.

In our previous work [5], we realized that, when using the finite element method for the discretization of the continuum model, matching the displacements $\mathrm{R}_o u$ and $\Pi_o w$ or/and the associated strains $(\mathrm{R}_o u)'$ and $(\Pi_o w)'$ at every point on the overlap region yielded erroneous results as soon as the mesh size was chosen smaller than the size of the representative volume element. In that case, the solution of the continuum model would indeed lock itself to the solution of the particle model. Our objective in this work is to define a formulation that is independent of the finite element mesh size.

In view of homogenization, the continuum model is derived by matching strain averages computed from the two models. An obvious choice is then to match the average of $(\mathrm{R}_o u)'$ with the average of $(\Pi_o w)'$ over a representative volume element, and in order to constrain rigid body motions, to match the average of the displacements $\mathrm{R}_o u$ and $\Pi_o w$ over the overlap Ω_o. Definition of these averages is straightforward except at the boundaries of Ω_o. We thus propose to define the averaging operators as follows, where the size of the RVE is denoted by ξ (see Fig. 7). Let $v \in H^1(\Omega_o)$, then

$$v^*(x) = \begin{cases} \dfrac{1}{\xi}\displaystyle\int_{x_a}^{x_a+\xi} v'dy = \dfrac{v(x_a+\xi)-v(x_a)}{\xi}, & \forall x \in [x_a, x_a+\xi/2], \\ \dfrac{1}{\xi}\displaystyle\int_{x-\xi/2}^{x+\xi/2} v'dy = \dfrac{v(x+\xi/2)-v(x-\xi/2)}{\xi}, & \forall x \in (x_a+\xi/2, x_b-\xi/2), \\ \dfrac{1}{\xi}\displaystyle\int_{x_b-\xi}^{x_b} v'dy = \dfrac{v(x_b)-v(x_b-\xi)}{\xi}, & \forall x \in [x_b-\xi/2, x_b]. \end{cases} \tag{21}$$

We also introduce the average[1] of a function $v \in H^1(\Omega_o)$ on Ω_o as:

$$\overline{v} = \frac{1}{|\Omega_o|}\int_{\Omega_o} v dx. \tag{22}$$

[1] In what follows, averages on Ω_o will always be denoted by a bar over the corresponding quantity.

Notice that the averaging operators $(\cdot)^*$ and $\overline{(\cdot)}$ are linear operators. As a result, the mismatch on overlap Ω_o between the solutions of the continuum and particle models can be measured as:

$$\begin{aligned}\mathscr{M}(\mathrm{R}_o u - \Pi_o w) &= \beta_0 \left|\overline{\mathrm{R}_o u} - \overline{\Pi_o w}\right|^2 + \beta_1 \int_{\Omega_o} \left|(\mathrm{R}_o u)^* - (\Pi_o w)^*\right|^2 dx \\ &= \beta_0 \left|\overline{(\mathrm{R}_o u - \Pi_o w)}\right|^2 + \beta_1 \int_{\Omega_o} \left|(\mathrm{R}_o u - \Pi_o w)^*\right|^2 dx,\end{aligned} \tag{23}$$

where (β_0, β_1) are non-negative weight parameters chosen such that the terms in above expression are of the same unit or dimensionless.

Remark 4. We readily observe that $\mathscr{M}$ defines a seminorm on $H^1(\Omega_o)$ as it is positive but not necessarily definite. Indeed, there exist non-vanishing functions $\mu \in H^1(\Omega_o)$ such that $\mathscr{M}(\mu) = 0$. Such functions are simply those that satisfy $\overline{\mu} = 0$ and $\mu^*(x) = 0$, $\forall x \in \Omega_o$. Let us introduce the subspace M_0 of $H^1(\Omega_o)$ as:

$$M_0 = \{\mu \in H^1(\Omega_o) : \ \overline{\mu} = 0 \text{ and } \mu^*(x) = 0, \ \forall x \in \Omega_o\}. \tag{24}$$

Functions in M_0 are those that are continuous with zero-mean and that are ξ-periodic on Ω_o. Let us restrict ourselves to the case where Ω_o exactly covers one RVE. Functions in $H^1(\Omega_o)$ can be represented in terms of Fourier Series as:

$$\mu(x) = a_0 + a_1 x + \sum_{k=1}^{\infty} b_k \sin k\pi \frac{x - x_a}{\xi}, \tag{25}$$

where a_0, a_1, and b_k are real numbers. Note that the family of functions $\sin k\pi(x - x_a)/\xi$ is linearly independent and complete in $H_0^1(\Omega_o)$ [1]. We then have two cases:

1. For k even, we observe that the functions $\mu(x) = \sin k\pi(x - x_a)/\xi$ have all zero mean, are ξ-periodic, and satisfy $\mu(x_b) = \mu(x_a) = 0$.
2. For k odd, we can show that the functions:

$$\mu(x) = \sin\left(k\pi \frac{x - x_a}{\xi}\right) - \frac{2}{k\pi} \tag{26}$$

have zero mean and are ξ-periodic. However, these functions do not necessarily vanish at the endpoints of Ω_o.

Therefore, the functions μ_0 in M_0 can be represented by linear combinations in the form:

$$\mu_0(x) = \sum_{k=1}^{\infty} b_k \left[\sin\left(2k\pi \frac{x - x_a}{\xi}\right)\right] + c_k \left[\sin\left((2k-1)\pi \frac{x - x_a}{\xi}\right) - \frac{2/\pi}{(2k-1)}\right]. \tag{27}$$

It follows that any function in $H^1(\Omega_o)$ can be expanded as:

$$\mu(x) = a_0 + a_1 x + \mu_0(x), \tag{28}$$

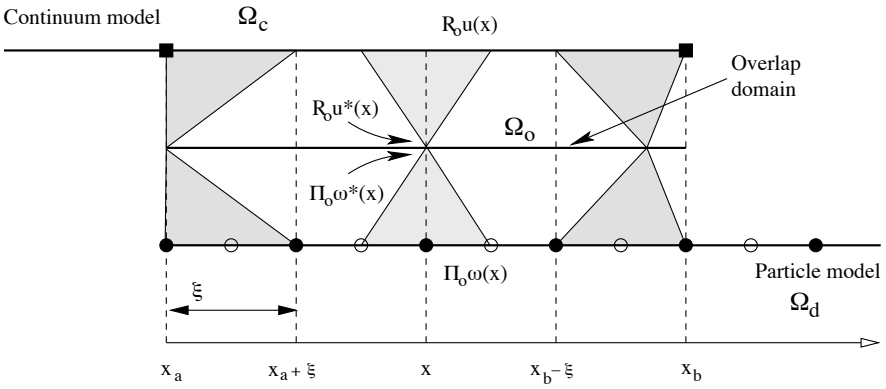

Fig. 7 Domain for the definition of the averaging operator.

where a_0 and a_1 are real numbers (that may take different values than those in (25)) and μ_0 is given by (27). Note that $\mathscr{M}$ now defines a norm on the quotient space $H^1(\Omega_o)/M_0$.

3.3 Formulation of the Coupled Problem

Let $V_c = \left\{ v \in H^1(\Omega_c) : \; v(0) = 0 \right\}$ and $V_d = \left\{ z \in \mathbb{R}^{m+1} \right\}$ be the vector spaces of test functions for the continuum and discrete models, respectively. The norms on V_c and V_d are chosen as:

$$\|v\|_{V_c} = \sqrt{\int_{\Omega_c} E|v'|^2 dx} \qquad \text{and} \qquad \|z\|_{V_d} = \sqrt{|z|^2_{V_d} + \delta|\overline{z}|^2}, \tag{29}$$

where we have introduced the seminorm $|\cdot|_{V_d}$ on V_d and average of z on Ω_o as:

$$|z|_{V_d} = \sqrt{\sum_{i=1}^{m} k_i (z_i - z_{i-1})^2} \qquad \text{and} \qquad \overline{z} = \frac{1}{|\Omega_o|} \sum_{i=1}^{m_o} l_i \frac{z_i + z_{i-1}}{2} = \overline{\Pi_o z}, \tag{30}$$

with δ a dimensionally consistent weighting constant that we define below. The vector space for the Lagrange multipliers and associated norm are given as $M = H^1(\Omega_o)/M_0$ and:

$$\|\mu\|_M = \sqrt{\beta_0 |\overline{\mu}|^2 + \beta_1 \int_{\Omega_o} |\mu^*|^2 dx} = \sqrt{\beta_0 |\overline{\mu}|^2 + \beta_1 \|\mu^*\|^2_{L^2(\Omega_o)}}, \tag{31}$$

with associated inner product:

$$(\lambda,\mu)_M = \beta_0 \overline{\lambda}\,\overline{\mu} + \beta_1 \int_{\Omega_o} \lambda^* \mu^* dx. \tag{32}$$

We also define the bilinear form $b(\cdot,\cdot)$ on $M \times X$ such that:

$$b(\mu, V) = (\mu, \mathrm{R}_o v - \Pi_o z)_M, \tag{33}$$

where, for the sake of simplicity in the notation, we have introduced the product space $X = V_c \times V_d$ with pairs of X denoted, for example, as $U = (u,w)$, $V = (v,z)$, and with norm:

$$\|V\|_X = \sqrt{\|v\|_{V_c}^2 + \|z\|_{V_d}^2}. \tag{34}$$

We now define the kernel space of $b(\cdot,\cdot)$ as the subspace of X such that:

$$X_0 = \{V \in X : \; b(\mu, V) = 0, \; \forall \mu \in M\}. \tag{35}$$

The coupled problem consists in finding $U \in X$ such that U minimizes the total energy and satisfies the constraint $\|\mathrm{R}_o u - \Pi_o w\|_M = 0$, i.e.

$$\hat{\mathscr{E}}(U) = \hat{\mathscr{E}}_c(u) + \hat{\mathscr{E}}_d(w) = \min_{\substack{V \in X \\ \|\mathrm{R}_o v - \Pi_o z\|_M = 0}} \left(\hat{\mathscr{E}}_c(v) + \hat{\mathscr{E}}_d(z) \right). \tag{36}$$

The minimization problem (36) can be recast into the following saddle point problem:

$$\boxed{\text{Find } U \in X,\, \lambda \in M \text{ such that} \quad L(U,\lambda) = \inf_{V \in X} \sup_{\mu \in M} L(V,\mu),} \tag{37}$$

where the Lagrangian reads:

$$L(V,\mu) = \hat{\mathscr{E}}_c(v) + \hat{\mathscr{E}}_d(z) + (\mu, \mathrm{R}_o v - \Pi_o z)_M = \frac{1}{2} a(V,V) - l(V) + b(\mu, V), \tag{38}$$

with

$$\begin{aligned} a(U,V) &= \int_{\Omega_c} \alpha_c E u' v' dx + \sum_{i=1}^{m} \alpha_i k_i (w_i - w_{i-1})(z_i - z_{i-1}), \\ l(V) &= f z_m. \end{aligned} \tag{39}$$

The coupled problem can then be recast in mixed form as:

$$\boxed{\begin{aligned} &\text{Find } U \in X,\, \lambda \in M \text{ such that:} \\ &\qquad a(U,V) + b(\lambda, V) = l(V), \quad \forall V \in X, \\ &\qquad\qquad b(\mu, U) = 0, \quad \forall \mu \in M. \end{aligned}} \tag{40}$$

We analyze below the mathematical properties of this coupled problem.

4 Mathematical Analysis of the Coupling Method

The main objective of this section is to show that Problem (40) is well-posed for $\beta_0 > 0$ and $\beta_1 > 0$. We present here a detailed proof and explicitly derive the bounding constants associated with the problem. Proofs of continuity of the forms $a(\cdot,\cdot)$ and $l(\cdot)$ were shown in [5]. We show below that the coupling term $b(\cdot,\cdot)$ is continuous and satisfies the Babuška-Brezzi condition and that form $a(\cdot,\cdot)$ is coercive. For simplicity of the proofs, we shall consider in this section that the overlap region Ω_o exactly coincides with one RVE.

Lemma 1 (Continuity of b). *Let $b(\cdot,\cdot)$ be as defined in* (32)*. Then, for all $\mu \in M$, $V = (v,z) \in X$, there exists a constant $M_b > 0$ such that:*

$$|b(\mu,V)| \leq M_b \|\mu\|_M \|V\|_X,$$

with

$$M_b = \sqrt{\beta_0 \left(\frac{|\Omega_c|^2}{2E|\Omega_o|} + \frac{1}{\delta} \right) + \beta_1 \left(\frac{1}{E} + \frac{1}{\min_i k_i l_i} \right)}, \tag{41}$$

where $\min_i$ *means the minimum over all values indexed by $i = 1,2,\ldots,m_o$.*

Proof. Let $\mu \in M$ and $V \in X$, such that $\mathrm{R}_o v \in M$ and $\Pi_o z \in M$. From the definition of the bilinear form $b(\cdot,\cdot)$ (32) and by using Cauchy-Schwarz, we have:

$$|b(\mu,V)| = (\mu, \mathrm{R}_o v - \Pi_o z)_M \leq \|\mu\|_M \|\mathrm{R}_o v - \Pi_o z\|_M \leq \|\mu\|_M (\|\mathrm{R}_o v\|_M + \|\Pi_o z\|_M).$$

Now, by definition of the norm, we have

$$\|\mathrm{R}_o v\|_M^2 = \beta_0 \overline{\mathrm{R}_o v}^2 + \beta_1 \|(\mathrm{R}_o v)^*\|_{L^2(\Omega_o)}^2. \tag{42}$$

Then, using Lemma A-2 in [5], the fact that $|\Omega_c| \geq |\Omega_o|$, and Poincaré inequality, we get:

$$\overline{\mathrm{R}_o v}^2 \leq \frac{1}{|\Omega_o|} \|\mathrm{R}_o v\|_{L^2(\Omega_o)}^2 \leq \frac{1}{|\Omega_o|} \|v\|_{L^2(\Omega_c)}^2 \leq \frac{|\Omega_c|^2}{2E|\Omega_o|} \|v\|_{V_c}^2. \tag{43}$$

For the other term, since $\mathrm{R}_o v \in M$, $\mathrm{R}_o v$ is linear on the RVE, and by assumption, on Ω_o. Then $(\mathrm{R}_o v)'$ is constant on Ω_o and it implies that $(\mathrm{R}_o v)^* = (\mathrm{R}_o v)'$, $\forall x \in \Omega_o$. It follows that:

$$\|(\mathrm{R}_o v)^*\|_{L^2(\Omega_o)}^2 = \|(\mathrm{R}_o v)'\|_{L^2(\Omega_o)}^2 = |(\mathrm{R}_o v)|_{H^1(\Omega_o)}^2 \leq |v|_{H^1(\Omega_c)}^2 = \frac{1}{E} \|v\|_{V_c}^2. \tag{44}$$

Then,

$$\|\mathrm{R}_o v\|_M \leq \|v\|_{V_c} \sqrt{\frac{\beta_0 |\Omega_c|^2}{2E|\Omega_o|} + \frac{\beta_1}{E}}. \tag{45}$$

In the same way, since $\Pi_o z$ is linear, we have

$$\|\Pi_o z\|_M^2 = \beta_0 \overline{\Pi_o z}^2 + \beta_1 \|(\Pi_o z)^*\|_{L^2(\Omega_o)}^2 = \beta_0 \bar{z}^2 + \beta_1 \|(\Pi_o z)'\|_{L^2(\Omega_o)}^2, \tag{46}$$

and

$$\begin{aligned} \|(\Pi_o z)'\|_{L^2(\Omega_o)}^2 &= \int_{\Omega_o} (\Pi_o z)'^2 dx = \sum_{i=1}^{m_o} l_i \left(\frac{z_i - z_{i-1}}{l_i} \right)^2 \\ &= \sum_{i=1}^{m_o} \frac{1}{k_i l_i} k_i (z_i - z_{i-1})^2 \leq \left(\min_i k_i l_i \right)^{-1} |z|_{V_d}^2. \end{aligned} \tag{47}$$

Therefore,

$$\|\Pi_o z\|_M^2 \leq \frac{\beta_0}{\delta} \delta \bar{z}^2 + \frac{\beta_1}{\min_i k_i l_i} |z|_{V_d}^2 \leq \left(\frac{\beta_0}{\delta} + \frac{\beta_1}{\min_i k_i l_i} \right) \|z\|_{V_d}^2. \tag{48}$$

We combine above results and find

$$M_b = \sqrt{\beta_0 \left(\frac{|\Omega_c|^2}{2E|\Omega_o|} + \frac{1}{\delta} \right) + \beta_1 \left(\frac{1}{E} + \frac{1}{\min_i k_i l_i} \right)}, \tag{49}$$

which completes the proof. □

Lemma 2 (Inf-sup condition for b). *Let $\beta_1 > 0$. Then, with above notation and definitions, there exists a constant $\gamma_b > 0$ such that:*

$$\inf_{\mu \in M} \sup_{V \in X} \frac{|b(\mu, V)|}{\|\mu\|_M \|V\|_X} \geq \gamma_b,$$

with

$$\gamma_b = \min \left(\sqrt{\frac{\beta_0}{2\delta}}, \sqrt{\frac{2\beta_1}{2E + \delta|\Omega_o|}} \right).$$

Proof. Let $\mu \in M \subset H^1(\Omega_o)$. It is sufficient to construct a pair $\hat{V} \in X$ such that

$$\sup_{V \in X} \frac{|b(\mu, V)|}{\|V\|_X} \geq \frac{|b(\mu, \hat{V})|}{\|\hat{V}\|_X} \geq \gamma_b \|\mu\|_M. \tag{50}$$

Since $M \subset H^1(\Omega_o)$, $\mu(x_a)$ is well defined and denoted by μ_a. We introduce the function $\hat{\mu}(x) = \mu(x) - \mu_a$ on $H^1(\Omega_o)$ and observe that $\hat{\mu}(x_a) = \mu(x_a) - \mu_a = 0$. Let $\hat{v} \in V_c$ such that $\hat{v} = \hat{\mu}$ on Ω_o and $\hat{v} = 0$ on $\Omega_c \backslash \Omega_o$ and let $\hat{z} \in V_d$ such that $\hat{z}_i = -\mu_a, \forall i = 1, \ldots, m$. Thus, taking $\hat{V} = (\hat{v}, \hat{z})$, we have:

$$\frac{|b(\mu, \hat{V})|}{\|\hat{V}\|_X} = \frac{|(\mu, \mathrm{R}_o \hat{v} - \Pi_o \hat{z})_M|}{\|(\hat{v}, \hat{z})\|_X} = \frac{|(\mu, \mu - \mu_a + \mu_a)_M|}{\|(\hat{v}, \hat{z})\|_X} = \frac{\|\mu\|_M^2}{\|(\hat{v}, \hat{z})\|_X}. \tag{51}$$

It suffices to show that $\|\mu\|_M / \|(\hat{v}, \hat{z})\|_X$ is greater than a positive constant independent of μ. We have

$$\begin{aligned}\|(\hat{v},\hat{z})\|_X^2 &= \|\hat{v}\|_{V_c}^2 + \|\hat{z}\|_{V_d}^2 = \int_{\Omega_o} E|\hat{v}'|^2 dx + |\hat{z}|_{V_d}^2 + \delta|\bar{\hat{z}}|^2 \\ &= \delta\mu_a^2 + \int_{\Omega_o} E|\mu'|^2 dx = \delta\mu_a^2 + \int_{\Omega_o} E|\mu^*|^2 dx,\end{aligned} \tag{52}$$

where we have used the fact that μ is linear on Ω_o, i.e. μ' is constant and $\mu' = \mu^*$. Then, rewriting $\mu = \mu'(x - x_a) + \mu_a$ and taking the average, we also have:

$$\mu_a = \bar{\mu} - \frac{1}{2}|\Omega_o|\mu', \tag{53}$$

and

$$\mu_a^2 \leq 2\overline{\mu}^2 + \frac{1}{2}|\Omega_o|^2(\mu')^2 = 2\overline{\mu}^2 + \frac{1}{2}|\Omega_o| \int_{\Omega_o} |\mu^*|^2 dx. \tag{54}$$

It follows that:

$$\begin{aligned}\|(\hat{v},\hat{z})\|_X^2 &\leq 2\delta\overline{\mu}^2 + \left(\frac{2E + \delta|\Omega_o|}{2}\right) \int_{\Omega_o} |\mu^*|^2 dx \\ &\leq \max\left(\frac{2\delta}{\beta_0}, \left(\frac{2E + \delta|\Omega_o|}{2\beta_1}\right)\right) \|\mu\|_M^2,\end{aligned} \tag{55}$$

and we conclude that

$$\frac{\|\mu\|_M}{\|(\hat{v},\hat{z})\|_X} \geq \min\left(\sqrt{\frac{\beta_0}{2\delta}}, \sqrt{\frac{2\beta_1}{2E + \delta|\Omega_o|}}\right), \tag{56}$$

which completes the proof. □

We now show the coercivity of a in the case where $\alpha_c = \alpha_d = 1/2$ on Ω_o. We believe that the result also holds when α_c is a continuous piecewise linear function but are not able to provide here a rigorous proof.

Lemma 3 (Coercivity of a). *Let $\alpha_c = \alpha_d = 1/2$. Then, with above notation and definitions, there exists a constant $\gamma_a > 0$ such that:*

$$\begin{cases} \inf\limits_{U\in X_0} \sup\limits_{V\in X_0} \dfrac{|a(U,V))|}{\|U\|_X \|V\|_X} > \gamma_a, \\ \sup\limits_{U\in X_0} a(U,V) > 0, \qquad \forall V \in X_0, V \neq 0, \end{cases} \tag{57}$$

with

$$\gamma_a = \frac{1}{2} \min_i \left(\frac{E}{k_i l_i}\right) \min_i \left(\frac{k_i l_i}{E}\right) \min\left(\frac{1}{2}, \frac{E}{\delta}\frac{|\Omega_o|}{|\Omega_c|^2}\right), \tag{58}$$

where $\min\limits_i$ *means the minimum over all values indexed by* $i = 1, 2, \ldots, m_o$.

Proof. It suffices to show that $a(\cdot,\cdot)$ is coercive on X_0. Let $V = (v,z) \in X_0$. By definition of the bilinear form, and the fact that $\alpha_c = 1$ on $\Omega_c \backslash \Omega_o$ and $\alpha_d = 1$ on

$\Omega_d \backslash \Omega_o$, we have

$$\begin{aligned} a(V,V) &= \int_{\Omega_c} \alpha_c E|v'|^2\,dx + \sum_{i=1}^{m} \alpha_i k_i (z_i - z_{i-1})^2 \\ &= \int_{\Omega_c \backslash \Omega_o} E|v'|^2\,dx + \sum_{i=m_o+1}^{m} k_i (z_i - z_{i-1})^2 \\ &\qquad + \int_{\Omega_o} \alpha_c E|(\mathrm{R}_o v)'|^2\,dx + \sum_{i=1}^{m_o} \alpha_i k_i (z_i - z_{i-1})^2. \end{aligned} \tag{59}$$

We provide here a general approach to show the coercivity. We first decompose the overlap terms in above equation into the following contributions:

$$\begin{aligned} &\int_{\Omega_o} \alpha_c E|(\mathrm{R}_o v)'|^2\,dx + \sum_{i=1}^{m_o} \alpha_i k_i (z_i - z_{i-1})^2 \\ &\qquad = \frac{1}{2}\left(\int_{\Omega_o} \alpha_c E|(\mathrm{R}_o v)'|^2\,dx + \sum_{i=1}^{m_o} \alpha_i k_i (z_i - z_{i-1})^2 \right) \\ &\qquad + \frac{1}{2}\left(\int_{\Omega_o} \alpha_c E|(\mathrm{R}_o v)'|^2\,dx + \sum_{i=1}^{m_o} \alpha_i k_i (z_i - z_{i-1})^2 \right). \end{aligned} \tag{60}$$

Since $V \in X_0$, the functions v and vectors z satisfy:

$$b(\mu, V) = (\mu, \mathrm{R}_o v - \Pi_o z)_M = 0, \qquad \forall \mu \in M. \tag{61}$$

In other words, $\mathrm{R}_o v - \Pi_o z \in M_o$, meaning that $\overline{\mathrm{R}_o v} = \overline{\Pi_o z}$ and that $v(x_b) - v(x_a) = z_{m_o} - z_o$ (where we appeal again to the fact that Ω_o consists of just one representative volume element). Let $\mu_o = \mathrm{R}_o v - \Pi_o z$ with $\overline{\mu_o} = 0$ and $\mu_o(x_a) = \mu_o(x_b)$. We also introduce the parameter $\kappa = \min_i(k_i l_i)/E$ and recall from Remark 1 that $\kappa \leq 1$. We have:

$$\begin{aligned} \frac{1}{2}\int_{\Omega_o} \alpha_c E|(\mathrm{R}_o v)'|^2 dx &\geq \frac{\kappa}{2}\int_{\Omega_o} \alpha_c E|(\mathrm{R}_o v)'|^2 dx \\ &\geq \frac{\kappa}{2}\int_{\Omega_o} \alpha_c E|(\Pi_o z)' + \mu_o'|^2 dx \\ &\geq \frac{\kappa}{2}\int_{\Omega_o} \alpha_c E|(\Pi_o z)'|^2 dx + \frac{\kappa}{2}\int_{\Omega_o} \alpha_c E|\mu_o'|^2 dx + \kappa \int_{\Omega_o} \alpha_c E(\Pi_o z)'\mu_o' dx. \end{aligned} \tag{62}$$

Using the fact that:

$$(\Pi_o z)' = \frac{z_i - z_{i-1}}{l_i}, \qquad \forall x \in (x_{i-1}, x_i), \tag{63}$$

the first integral can be rewritten as:

$$\begin{aligned}\int_{\Omega_o} \alpha_c E|(\Pi_o z)'|^2 dx &= \sum_{i=1}^{m_o} \int_{x_i-1}^{x_i} \alpha_c E \left[\frac{z_i - z_{i-1}}{l_i}\right]^2 dx \\ &= \sum_{i=1}^{m_o} \frac{E}{k_i l_i} k_i (z_i - z_{i-1})^2 \left[\frac{1}{l_i}\int_{x_i-1}^{x_i} \alpha_c dx\right],\end{aligned} \tag{64}$$

and, using the definition of α_i, we get:

$$\int_{\Omega_o} \alpha_c E|(\Pi_o z)'|^2 dx \geq \min_i \left(\frac{E}{k_i l_i}\right) \sum_{i=1}^{m_o} (1-\alpha_i) k_i (z_i - z_{i-1})^2. \tag{65}$$

It follows that

$$\begin{aligned}\frac{1}{2}\int_{\Omega_o} \alpha_c E|(\mathrm{R}_o v)'|^2 dx \geq \frac{\kappa}{2} \min_i \left(\frac{E}{k_i l_i}\right) \sum_{i=1}^{m_o} (1-\alpha_i) k_i (z_i - z_{i-1})^2 \\ + \frac{\kappa}{2}\int_{\Omega_o} \alpha_c E|\mu_o'|^2 dx + \kappa \int_{\Omega_o} \alpha_c E(\Pi_o z)'\mu_o' dx.\end{aligned} \tag{66}$$

In the same way, we have:

$$\begin{aligned}\frac{1}{2}\sum_{i=1}^{m_0} \alpha_i k_i (z_i - z_{i-1})^2 &\geq \frac{\kappa}{2}\int_{\Omega_o} (1-\alpha_c) E|(\Pi_o z)'|^2 dx \\ &\geq \frac{\kappa}{2}\int_{\Omega_o} (1-\alpha_c) E|(\mathrm{R}_o v)' - \mu_o'|^2 dx \\ &\geq \frac{\kappa}{2}\int_{\Omega_o} (1-\alpha_c) E|(\mathrm{R}_o v)'|^2 dx \\ &\quad + \frac{\kappa}{2}\int_{\Omega_o} (1-\alpha_c) E|\mu_o'|^2 dx - \kappa \int_{\Omega_o} (1-\alpha_c) E(\mathrm{R}_o v)'\mu_o' dx.\end{aligned} \tag{67}$$

Using (66) and (67) in (60), we obtain:

$$\begin{aligned}&\int_{\Omega_o} \alpha_c E|(\mathrm{R}_o v)'|^2 \, dx + \sum_{i=1}^{m_o} \alpha_i k_i (z_i - z_{i-1})^2 \\ &\quad \geq \frac{\kappa}{2}\left[\int_{\Omega_o} \alpha_c E|(\mathrm{R}_o v)'|^2 dx + \int_{\Omega_o} (1-\alpha_c) E|(\mathrm{R}_o v)'|^2 dx\right] \\ &\qquad + \frac{\kappa}{2}\int_{\Omega_o} (1-\alpha_c) E|\mu_o'|^2 dx - \kappa \int_{\Omega_o} (1-\alpha_c) E(\mathrm{R}_o v)'\mu_o' dx \\ &\qquad + \frac{\kappa}{2}\min_i \left(\frac{E}{k_i l_i}\right)\left[\sum_{i=1}^{m_o} \alpha_i k_i (z_i - z_{i-1})^2 + \sum_{i=1}^{m_o} (1-\alpha_i) k_i (z_i - z_{i-1})^2\right] \\ &\qquad + \frac{\kappa}{2}\int_{\Omega_o} \alpha_c E|\mu_o'|^2 dx + \kappa \int_{\Omega_o} \alpha_c E(\Pi_o z)'\mu_o' dx.\end{aligned} \tag{68}$$

Simplifying, we get:

$$\begin{aligned}
&\int_{\Omega_o} \alpha_c E|(\mathrm{R}_o v)'|^2\,dx + \sum_{i=1}^{m_o} \alpha_i k_i (z_i - z_{i-1})^2 \\
&\geq \frac{1}{2}\min_i\left(\frac{E}{k_i l_i}\right)\min_i\left(\frac{k_i l_i}{E}\right)\left[\int_{\Omega_o} E|(\mathrm{R}_o v)'|^2\,dx + \sum_{i=1}^{m_o} k_i (z_i - z_{i-1})^2\right] \\
&\quad + \frac{\kappa}{2}\int_{\Omega_o} E|\mu_o'|^2 dx - \kappa\int_{\Omega_o}(1-\alpha_c)E(\mathrm{R}_o v)'\mu_o' dx + \kappa\int_{\Omega_o}\alpha_c E(\Pi_o z)'\mu_o' dx.
\end{aligned} \tag{69}$$

We note that the last three terms, denoted by $\mathscr{K}$, can be combined as follows:

$$\begin{aligned}
\mathscr{K} &= \frac{\kappa}{2}\int_{\Omega_o}(2\alpha_c - 1)\,E\left[2(\mathrm{R}_o v)' - \mu_o'\right]\mu_o' dx \\
&= \frac{\kappa}{2}\int_{\Omega_o}(2\alpha_c - 1)\,E\left[|(\mathrm{R}_o v)'|^2 - |(\Pi_o z)'|^2\right]dx.
\end{aligned} \tag{70}$$

The goal would be to show that $\mathscr{K} \geq 0$ for all $(v,z) \in X_0$ for any admissible profile of α_c on Ω_o. Unfortunately, we are only able to date to prove that $\mathscr{K} = 0$ if $\alpha_c = 1/2$. It is not clear at this point whether the result would hold in the case where α_c is continuous piecewise linear.

Finally, setting $\alpha_c = 1/2$, we may proceed as follows:

$$\begin{aligned}
a(V,V) &\geq \int_{\Omega_c\setminus\Omega_o} E|v'|^2\,dx + \sum_{i=m_o+1}^{m} k_i(z_i - z_{i-1})^2 \\
&\quad + \frac{1}{2}\min_i\left(\frac{E}{k_i l_i}\right)\min_i\left(\frac{k_i l_i}{E}\right)\left[\int_{\Omega_o} E|v'|^2\,dx + \sum_{i=1}^{m_o} k_i(z_i - z_{i-1})^2\right] \\
&\geq \frac{1}{2}\min_i\left(\frac{E}{k_i l_i}\right)\min_i\left(\frac{k_i l_i}{E}\right)\left[\int_{\Omega_c} E|v'|^2\,dx + \sum_{i=1}^{m} k_i(z_i - z_{i-1})^2\right] \\
&\geq \gamma\left(\|v\|_{V_c}^2 + |z|_{V_d}^2\right),
\end{aligned} \tag{71}$$

where we have introduced the constant γ as:

$$\gamma = \frac{1}{2}\min_i\left(\frac{E}{k_i l_i}\right)\min_i\left(\frac{k_i l_i}{E}\right). \tag{72}$$

Applying first the Poincaré inequality, i.e.

$$a(V,V) \geq \gamma\left(\frac{1}{2}\|v\|_{V_c}^2 + \frac{E}{|\Omega_c|^2}\|v\|_{L^2(\Omega_c)}^2 + |z|_{V_d}^2\right), \tag{73}$$

and then Lemma A-2 in [5], as well as the fact that X_0 consists of those functions v and vectors z such that $\bar{v} = \overline{\Pi_o z} = \bar{z}$ on Ω_o, i.e.

$$\|v\|_{L^2(\Omega_c)}^2 \geq \|v\|_{L^2(\Omega_o)}^2 \geq \bar{v}^2|\Omega_o| = \bar{z}^2|\Omega_o|, \tag{74}$$

we finally obtain:

$$a(V,V) \geq \gamma \left(\frac{1}{2} \|v\|_{V_c}^2 + |z|_{V_d}^2 + \frac{E}{\delta} \frac{|\Omega_o|}{|\Omega_c|^2} \delta \bar{z}^2 \right) \geq \gamma \min \left(\frac{1}{2}, \frac{E}{\delta} \frac{|\Omega_o|}{|\Omega_c|^2} \right) \|V\|_X^2, \quad (75)$$

which completes the proof. □

From above lemmas, we may conclude that the Arlequin problem is well-posed as long as $\beta_0 > 0$ and $\beta_1 > 0$ (and restriction that $\alpha_c = 1/2$ on overlap domain).

5 Finite Element Formulation

We introduce in this section the finite element formulation of the coupled problem. Let V_c^h and M^h be finite element subspaces of the vector spaces V_c and M, respectively, and let X^h be the product space $X^h = V_c^h \times V_d$. The subspace V_c^h can be constructed as the space spanned by the piecewise linear continuous functions defined with respect to the set of nodes $x_i = ih$, $i = 0, \ldots, N^e$, where N^e denotes the number of elements in the mesh. In the case of M^h, we are clearly faced with several choices since the elements associated with V_c^h and M^h do not have to match. However, for the sake of simplicity, one possibility is to restrict ourselves to cases where each node of the mesh associated with M^h coincides either with a particle or with a node of V_c^h or both. However, M^h needs to be constructed in such a way that the condition $M^h \subset M = H^1(\Omega_o) \backslash M_0$ be satisfied, that is, we need to make sure that functions of M_0 are excluded from M^h. Let $\widetilde{M}^h$ be the vector space spanned by continuous piecewise linear functions defined on Ω_o and let h_M be the mesh size associated with $\widetilde{M}^h$ (assume a uniform grid here). If the overlap region consists of one RVE and if n_s denotes the number of springs in one RVE, we have been able to observe numerically that the number of modes in $\widetilde{M}^h \cap M_0$ is given by:

$$n_0 = \begin{cases} \dfrac{n_s l_i}{h_M} - 1, & \text{if } h_M < \xi, \\ 0, & \text{otherwise}, \end{cases} \quad (76)$$

where ξ is the size of the RVE and l_i is the equilibrium length of each bond (assumed constant here). It follows that a convenient way to construct the finite element space M^h is to consider continuous piecewise linear functions defined with respect to elements of size $h_M = \xi$ (or a multiple of ξ).

Finally, we introduce the notation $U_h = (u_h, w_h)$ and $V_h = (v_h, z)$. Then, Problem (40) is approximated as follows:

$$\boxed{\begin{array}{l} \text{Find } U_h \in X^h,\ \lambda_h \in M^h \text{ such that:} \\ \qquad a(U_h, V_h) + b(\lambda_h, V_h) = l(V_h), \quad \forall V_h \in X^h, \\ \qquad\qquad b(\mu_h, U_h) = 0, \quad \forall \mu_h \in M^h. \end{array}} \quad (77)$$

We note that although V_d is a finite-dimensional space and, consequently does not need to be discretized using finite elements, we will use the notation w_h to denote the solution of the particle model in (77) to emphasize that w_h directly depends on the choice of V_h and M_h. We can show that above problem is also well-posed when $\beta_0 > 0$, $\beta_1 > 0$, and $\alpha_c = 1/2$.

6 Numerical Results

6.1 One-Dimensional Numerical Results

In this section, we present some numerical experiments to illustrate our theoretical study of a one-dimensional coupled problem, i.e. a model of harmonic springs, with varying coefficients, coupled with a linear elastic bar, whose Young's modulus is determined by simple homogenization. Unless otherwise stated, we consider in the following experiments the domain $\Omega = (0,3)$. The continuum model is used in the subdomain $\Omega_c = (0,2)$ while the particle model is used in $\Omega_d = (1,3)$ and the weight coefficients α_c and α_d are chosen linear in the overlap domain. Moreover, the force f applied at $x = 3$ is chosen in such a way that the displacement at the right end of the domain, when using the continuum model everywhere in Ω, is equal to unity. We also restrict ourselves to the cases where the equilibrium lengths of the springs are all equal. We also recall that the discrete problem is well-posed if the mesh size used to discretize the Lagrange multiplier space is at least larger than (a multiple of) the size of the repesentative cell. Hence, in the following, the size of the elements used to define M^h is always taken equal to the size of the representative volume element.

6.1.1 Overlap Region Composed of One RVE

Let us start by studying the very simple case of an overlap domain composed of only one RVE. As the objective is to propose a method that is well suited to solve problems dealing with highly heterogeneous particle models, we study here the particle case of a periodic distribution of springs with two spring stiffness parameters for which it is straightforward to derive an equivalent continuum model. Thus, the particle model is chosen to be composed of $m = 4$ springs in Ω_d, i.e. five particles, and that the values of the spring stiffness are $k_1 = 100$ and $k_2 = 1$. The particle structure is then constructed, for m even, as:

$$k_{2j-1} = k_1, \qquad k_{2j} = k_2, \qquad \forall j = 1, \ldots, m/2. \tag{78}$$

The equilibrium length of each spring is chosen constant as $l = l_i = 0.5$ and the corresponding Young's modulus E is then given by:

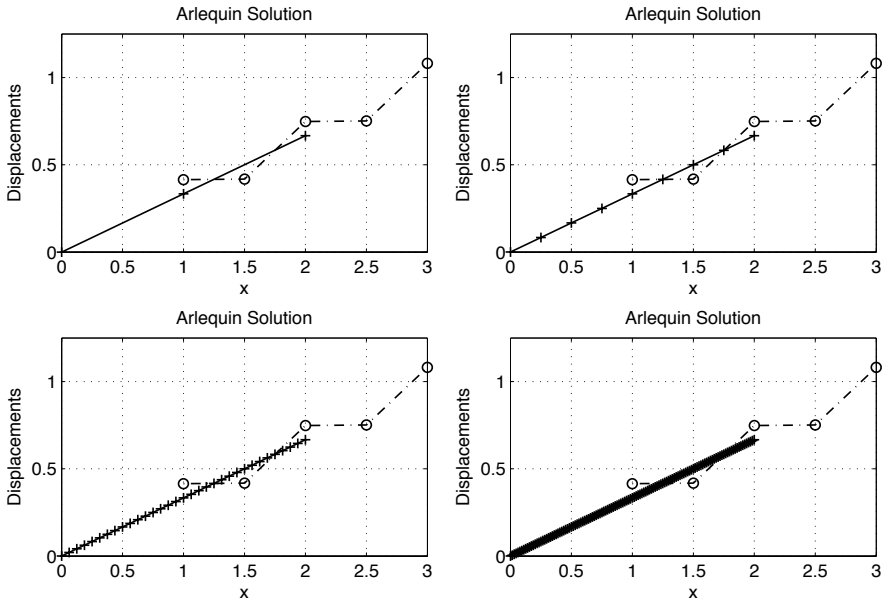

Fig. 8 Arlequin solution in case of one RVE in the overlap region for several mesh sizes.

$$E = \frac{k_1 k_2}{k_1 + k_2} 2l = \frac{100}{101} \times 2 \times 0.5 = 0.99010, \tag{79}$$

using the expression derived in (11). In the following set of experiments, we study the effect of the mesh size on the Arlequin solution. The Arlequin solutions for four different mesh sizes, namely $h = 2l$, $h = l/2$, $h = l/4$, and $h = l/32$, where h is the size of the elements for V_c^h, are shown in Fig. 8. As expected, the coupled solution is independent of the mesh size as the displacement z_m of the right end particle is equal for all cases to 1.08168. Notice however that z_m is different from unity, as one might have expected from the choice of the loading force f applied to particle m. This is simply due to the fact that the displacement of the particles is averaged around the continuum solution on the overlap region. If we average the particle solution in Ω_d, we would then obtain a displacement equal to unity since the slope of the continuum solution and that of the averaged particle solution are identical.

6.1.2 Overlap Region Composed of Several RVE's

We now repeat the same experiments in the case where the size of the overlap region is equal to the size of several RVEs. We keep the same periodic distribution as before, that is, the RVE is made of two springs with stiffness coefficients $k_1 = 100$ and $k_2 = 1$. We consider the case where the overlap region is composed of two RVEs and the particle structure is made of $m = 8$ springs ($l = 0.25$), and the case of

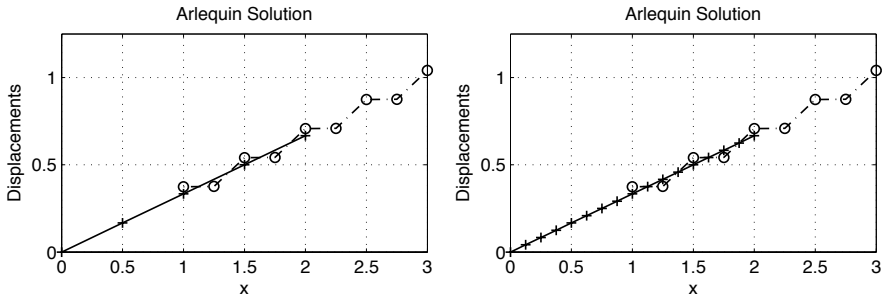

Fig. 9 Arlequin solution in case of two RVEs in the overlap region for two different mesh sizes.

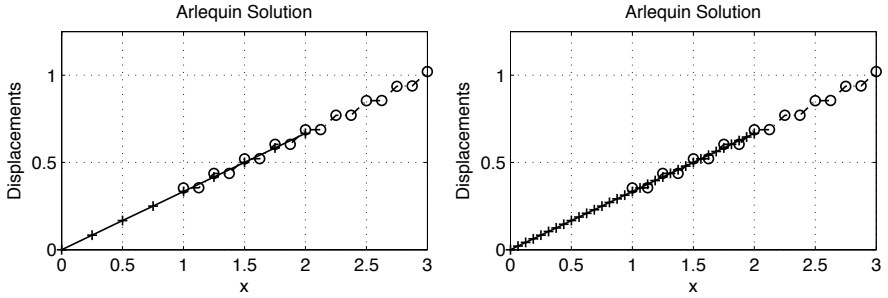

Fig. 10 Arlequin solution in case of four RVEs in the overlap region for two different mesh sizes.

four RVEs in the overlap region and a particle model composed of $m = 16$ springs ($l = 0.125$). For both cases, we compute the solutions on two different mesh sizes, namely $h = 2l$ and $h = l/2$, as shown in Figs. 9 and 10. We can see that the method produces the correct results as expected. The displacements at the right end particle are $z_m = 1.04084$ and $z_m = 1.02042$ in the case of two RVEs and four RVEs, respectively. These displacements get actually closer to unity since the smaller the equilibrium lengths are, the closer the particle solution gets to the continuum solution.

6.1.3 An Example with a Large Number of Particles

In more practical cases, we are interested in systems that are composed of many particles. The objective is to use the particle model around a tiny zone to model the small scale behavior of the material, and in the remaining zone, to use the continuum model in order to reduce the cost of the simulation. We consider here the case of the structure made of a chain of 1001 particles connected by 1000 springs in the domain $\Omega = (0,1)$, as shown in Fig. 11 . We define $\Omega_c = (0,0.8)$ and $\Omega_d = (0.796,1)$. We assume for the particle model a periodic distribution of four springs with spring constants $k_1 = 100$, $k_2 = 1$, $k_3 = 50$, and $k_4 = 10$, and equilibrium length $l = 0.001$,

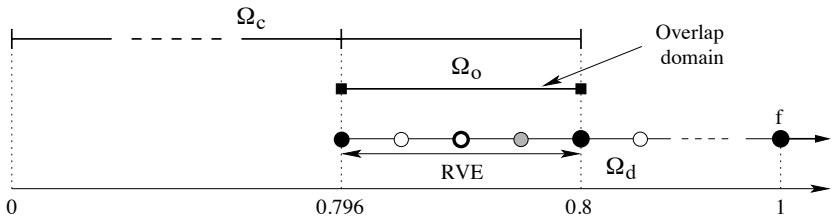

Fig. 11 Implementation of the Arlequin method on a system of 1001 particles.

for which we get the equivalent Young's modulus E as:

$$E = \left[\frac{1}{k_1^{-1}+k_2^{-1}+k_3^{-1}+k_4^{-1}}\right] 4l = \left[\frac{1}{0.01+1.00+0.02+0.10}\right] \times 4 \times 0.001, \tag{80}$$

that is, $E = 3.539823 \times 10^{-3}$. Notice that the definition of the geometry implies that the overlap domain Ω_o is made of just one representative cell. With the idea of considering a critical and practical experiment, we discretize Ω_c with a mesh made of two elements. The first element covers the continuum region $\Omega_c \backslash \Omega_o$ while the second element covers the whole overlap region Ω_o. The Arlequin solution is shown in Fig. 12. We observe that the large-scale displacement in the whole structure is perfectly linear and that the displacement at $x = 1$ is again closer to unity ($z_m = 0.99969$) than in the previous results since the equilibrium length of the springs is here reduced to $l = 0.001$. These results clearly demonstrate that we can consider an extreme configuration of a continuum model discretized with only two elements (one for the whole continuum region and one for the coupling zone) to deliver accurate simulations. In other words, only one element is sufficient to model the behavior of the material in $\Omega_c \backslash \Omega_o$ (since the model is linear) and one element to discretize the overlap region (composed of one RVE) is enough to couple the two models.

6.1.4 Simulation of a Defect

The goal in using the proposed coupling method is to replace the particle model by a continuum model in the region where only the large-scale contributions to the values of quantities of interest are significant and where the continuum model remains compatible with the particle model. The hope then is that the particle model would only be required in a small region of the whole domain, around a defect or a geometrical singularity for instance. We propose here to consider a one-dimensional structure, fixed at both extremities and subjected to a point force applied at the center particle (see Fig. 13), in which the stiffness coefficients in the middle bonds are purposely weakened as follows:

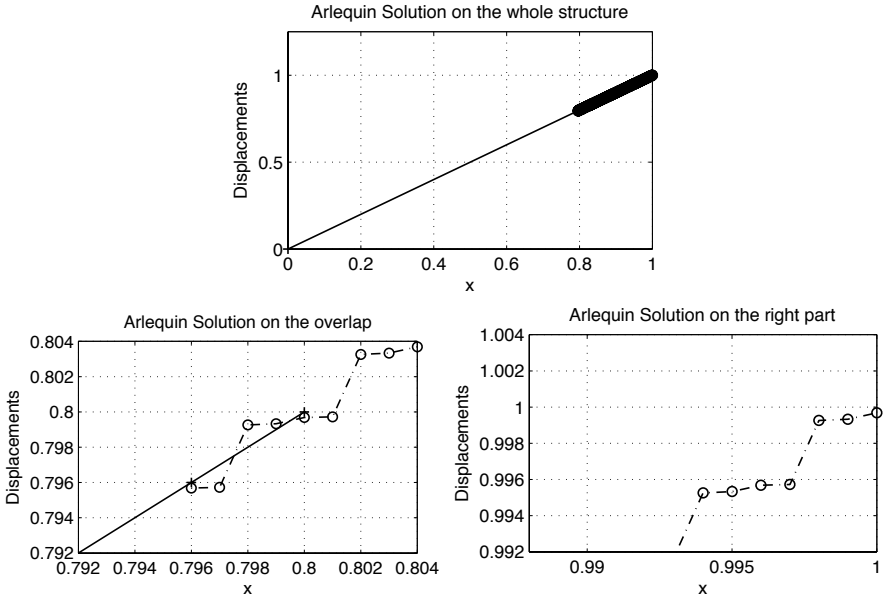

Fig. 12 Arlequin solution in case of a system with many particles using a mesh only composed of two elements.

$$k_i^* = k_i \left[\frac{1}{1 + 20e^{-5(x-L/2)^2}} \right], \tag{81}$$

where L is the length of the structure. The main objective here is to model a pseudo-defect in the chain of particles around which the continuum model is no longer compatible with the particle model. The domain is given by $\Omega = (0.0, 5.2)$, i.e. $L = 5.2$, and the particle model is kept only in the subdomain $\Omega_d = (1.4, 3.8)$. The equilibrium length of the bonds is set to $l = 0.1$. Furthermore, we assume that the particle model is defined as a periodic distribution of two spring stiffness parameters $k_1 = 100$ and $k_2 = 30$ along which the proposed defect is superimposed. The Young's modulus of the continuum model is computed by ignoring the defect in the particle model, i.e. by considering the stiffness coefficients k_i rather than k_i^*. Using (79), its value is found to be $E = 4.61538$. In order to study the influence of the position and size of the overlap region onto the Arlequin solution, we consider four different configurations of the coupling zones defined by the overlap regions $\Omega_{o,1} = (1.4, 1.4 + 0.2j)$ and $\Omega_{o,2} = (3.8 - 0.2j, 3.8)$, on the left and on the right of the particle model, respectively, with $j = 1, \ldots, 4$ (see Fig. 13). In other words, the size of the region in which the particle model is used is enlarged as the overlap regions are made of 4, 3, 2, and 1 RVE's by varying j from 4 to 1. Finally, the length of the elements is set to $h = 2l$ in $\Omega_c = \Omega_{c,1} \cup \Omega_{c,2}$.

The results are shown in Fig. 14. The first solution is obtained using $j = 4$ and the last one using $j = 1$. The maximum displacement, which corresponds to the

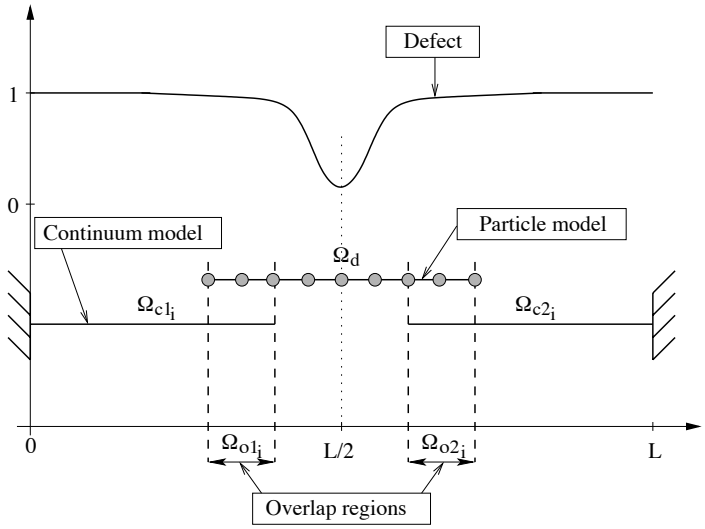

Fig. 13 Definition of the coupled model for the simulation of a defect.

displacement of the particle at the center, is reported for each configuration in Table 1. We observe that the approximations of the displacement become more accurate when the overlap regions are positioned away from the defect. This is due to the fact that the continuum model is not compatible with the particle model in the vicinity of the defect since the former is calibrated from the latter without taking the defect into account. However, in the case of the configuration with $j = 1$, the models become compatible with each other and the proposed coupling term provides an accurate solution around the defect with respect to the solution of the full particle model (not shown here).

Table 1 Maximum displacement for various values of the number of RVE's, n_{RVE}, in each overlap region.

n_{RVE}	Maximum Displacement
4	1.05137
3	1.12014
2	1.13450
1	1.13670

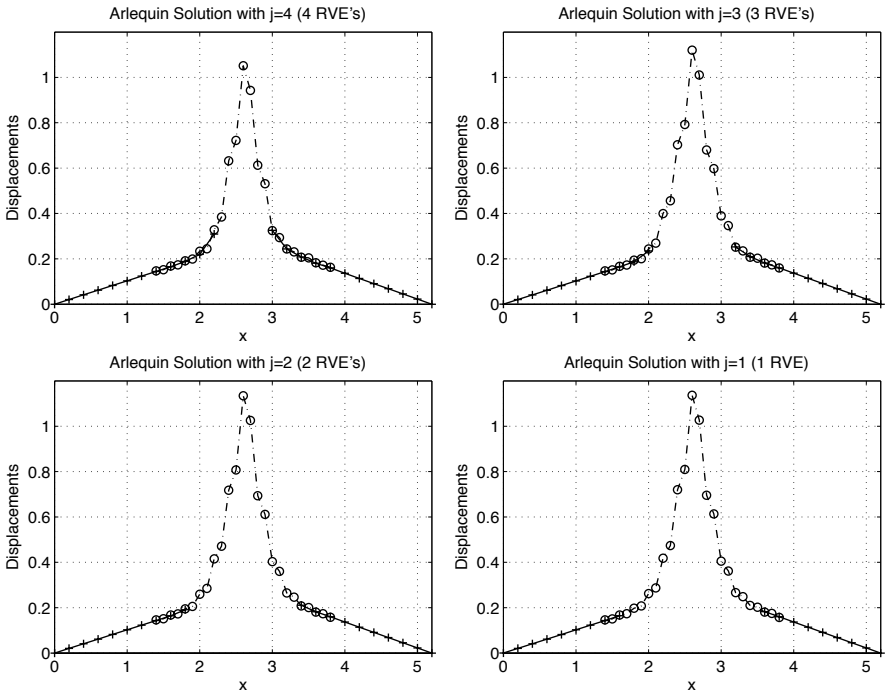

Fig. 14 Arlequin solutions obtained for different configurations of the coupling regions defined by $\Omega_{o,1} = (1.4, 1.4 + 0.2j)$ and $\Omega_{o,2} = (3.8 - 0.2j, 3.8)$, on the left and on the right of the particle model, respectively, with $j = 1, \ldots, 4$.

6.2 Two-Dimensional Numerical Results

In this section, we apply the Arlequin formulation using the new coupling operator to the case of two-dimensional problems. In particular, we consider a uniform lattice in which the interactions between particles are modeled in terms of harmonic springs. The particles are supposed to interact only with their nearest neighbors: in the x- and y-directions, the stiffness parameter for each bond is given by k while in the diagonal direction, the stiffness coefficient is set to k_d. The Representative Volume Element is easily identified here as the cell defined by four lattice sites since it represents the smallest substructure within the periodic structure. The RVE is utilized to compute the material coefficients (Young's modulus and Poisson's ratio) of the compatible linear elasticity model.

The system of interest is made of 11×11 particles and is subjected to a point force applied to the particle located at the center of the domain. For large values of the force, displacements in the vicinity of the centered particle are expected to vary rapidly, implying that the linear elasticity model would incorrectly predict the large associated strains. In this simple example, we choose to employ the particle model in the subdomain at the center of the domain, of size corresponding to four RVE's, and

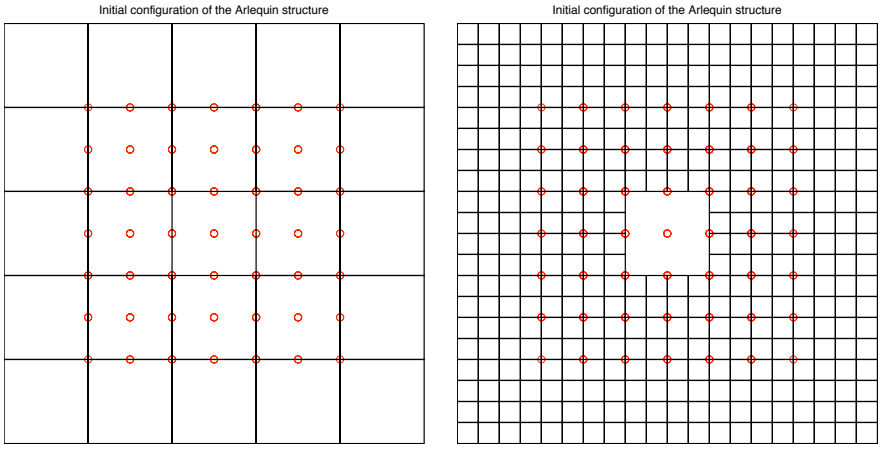

Fig. 15 Arlequin configuration of the coupled problem using a coarse mesh (left) and a fine mesh (right) for the discretization of the continuum model. The particle model is reduced to the subdomain in the center and the overlap region consists of a layer around the particle region.

to construct the overlap region as the layer around the particle region, of thickness corresponding to the size of two RVE's. The continuum model is selected in the remainder of the domain and is discretized using quadrilateral bilinear elements (see Fig. 15). Finally, the system is subjected to homogeneous Dirichlet boundary conditions along the boundary $\partial\Omega$.

In order to test the method, we consider in what follows a coarse mesh and a fine mesh: on the coarse mesh, the finite elements have a mesh size equal to the size of two RVE's for the discretization of the continuum solution and of the Lagrange multiplier as shown on the left of Fig. 15; on the fine mesh, the elements are half the size of one RVE for the continuum solution and twice the size of one RVE for the Lagrange multiplier as shown on the right of Fig. 15.

Finally, we compute two Arlequin solutions on each of the two meshes: in the first Arlequin formulation, the coupling term is defined in terms of the H^1 norm as described in [5] while in the second formulation, the coupling term is defined using the proposed averaging operator. In both formulations, the weighting coefficients are chosen constant on the overlap region and equal to one half. On the coarse mesh, the two solutions are identical as expected (see Fig. 16). The fact that large elements are used in the formulation is equivalent to an averaging over a representative volume element. However, the two solutions are different on the fine mesh (see Fig. 17). This is due to the locking phenomenon in the case of the H^1 norm coupling, that is, the displacements of the continuum solution lock themselves to the displacements of the particle solution on the overlap region. A better approximation, better in the sense that the solution is closer to that of the full particle model, is therefore obtained using the formulation involving the averaging operator.

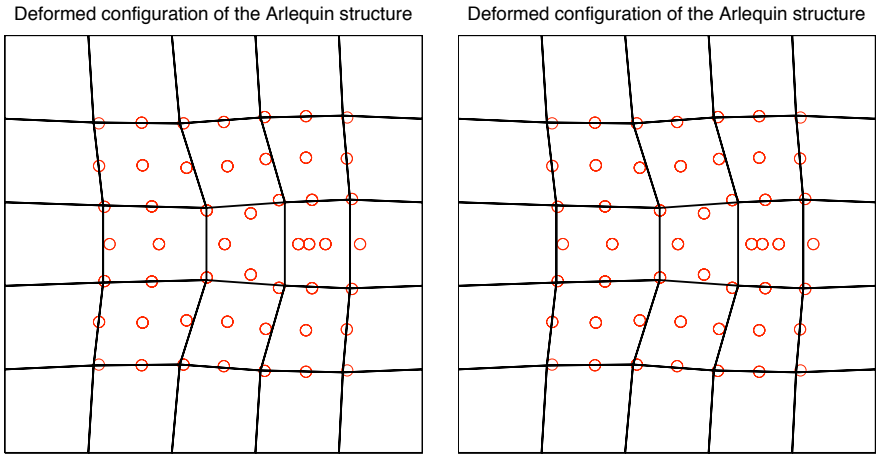

Fig. 16 Deformed configuration on coarse mesh using the Arlequin framework: (Left) the coupling term is defined in terms of the H^1 norm; (Right) the coupling term is defined in terms of the proposed averaging operator. The two solutions are identical as expected.

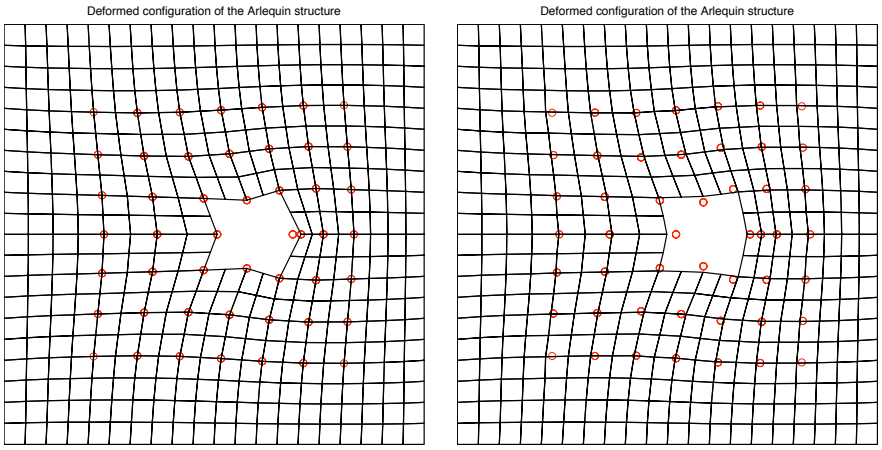

Fig. 17 Deformed configuration on fine mesh using the Arlequin framework: (Left) the coupling term is defined in terms of the H^1 norm; (Right) the coupling term is defined in terms of the proposed averaging operator. The two solutions are now different.

7 Conclusion

We have presented in this paper a new expression for the coupling term when blending a particle model with a continuum model using the Arlequin framework. The coupling method belongs to the family of concurrent methods for solving multi-scale problems. It constitutes an improved version of a previously proposed coupling method, described in [5], which had the major drawback of being mesh-dependent

in the sense that meshes had to be carefully selected in order to obtain the intended solution of the problem. In particular, it was shown that the method produced satisfactory results as long as the mesh size of the finite elements used to discretize the Lagrange multiplier space was at least larger than (a multiple of) the size of the representative cell defined to calibrate the parameter(s) of the continuum model. In the new coupling method, the selection of meshes used to discretize the continuum solution and the Lagrange multiplier is immediately determined from the formulation of the continuous problem.

The new coupling term is constructed in terms of an averaging operator defined on a representative cell. The cell size determines in some sense the scale at which the continuum model and particle model can exchange information. Indeed, the parameters of the continuum model are usually identified through homogenization from the solution of the particle model computed on one representative cell. We have shown here that the resulting coupled problem is mathematically well-posed and that its discretization by the finite element method provides approximations that converge to the exact solution of the problem as the mesh size goes to zero. We have illustrated on one- and two-dimensional examples that the proposed approach is well suited for problems in which the bonds between particles are heterogeneously distributed. Systems in the present study were considered periodic as compatible continuum models can straightforwardly be derived through classical homogenization techniques.

The study of coupling methods based on the Arlequin framework for blending particle and continuum models is by no means complete. This work only represents one step in the development of general coupling methods. In particular, it would be interesting to investigate the extension of this formulation to stochastic systems for which the notion of representative volume element is not well defined. A preliminary study on this subject is described in [15] based on the coupling method proposed in [5]. Our objective in the near future would be to reconsider stochastic particle systems using the new averaging operator for coupling the continuum and particle models.

Acknowledgement

Support of this work by DOE under contract DE-FG02-05ER25701 is gratefully acknowledged. The second author, Robin Bouclier, would like also to thank ICES for hosting him for his internship during the Summer of 2009.

References

1. Babuška, I., Banerjee, U., Osborn, J.E.: On principles for the selection of shape functions for the generalized finite element method. Computer Methods in Applied Mechanics and Engineering **191**(49), 5595–5629 (2002)

2. Badia, S., Bochev, P., Fish, J., Gunzburger, M., Lehoucq, R., Nuggehally, M., Parks, M.: A force-based blending model for atomistic-to-continuum coupling. International Journal for Multiscale Computational Engineering **5**, 387–406 (2007)
3. Badia, S., Parks, M., Bochev, P., Gunzburger, M., Lehoucq, R.: On atomistic-to-continuum (atc) coupling by blending. Multiscale Modeling and Simulation **7**, 381–406 (2008)
4. Bauman, P.T.: Adaptive multiscale modeling of polymeric materials using goal-oriented error estimation, arlequin coupling, and goals algorithms. Ph.D. thesis, The University of Texas at Austin (2008)
5. Bauman, P.T., Ben Dhia, H., Elkhodja, N., Oden, J.T., Prudhomme, S.: On the application of the Arlequin method to the coupling of particle and continuum models. Computational Mechanics **42**, 511–530 (2008)
6. Bauman, P.T., Oden, J.T., Prudhomme, S.: Adaptive multiscale modeling of polymeric materials: Arlequin coupling and goals algorithms. Computer Methods in Applied Mechanics and Engineering **198**, 799–818 (2008)
7. Belytschko, T., Xiao, S.P.: Coupling methods for continuum model with molecular model. International Journal for Multiscale Computational Engineering **1**(1), 115–126 (2003)
8. Ben Dhia, H.: Multiscale mechanical problems: the Arlequin method. Comptes Rendus de l'Académie des Sciences Paris Série IIB **326**(12), 899–904 (1998)
9. Ben Dhia, H.: Global local approaches: the Arlequin framework. European Journal of Computational Mechanics **15**(1–3), 67–80 (2006)
10. Ben Dhia, H., Elkhodja, N.: Coupling of atomistic and continuum models in the Arlequin framework. In: Proceedings of the 8eme Congrès de Mécanique, pp. 133–135. El Jadida, Maroc (2007)
11. Ben Dhia, H., Rateau, G.: Mathematical analysis of the mixed Arlequin method. Comptes Rendus de l'Académie des Sciences Paris Série I **332**, 649–654 (2001)
12. Ben Dhia, H., Rateau, G.: Application of the Arlequin method to some structures with defects. Revue Européenne des Eléments Finis **332**, 649–654 (2002)
13. Ben Dhia, H., Rateau, G.: The Arlequin method as a flexible engineering design tool. Int. J. Numer. Meth. Engng. **62**(11), 1442–1462 (2005)
14. Broughton, J.Q., Abraham, F.F., Bernstein, N., Kaxiras, E.: Concurrent coupling of length scales: Methodology and application. Phys. Rev. B **60**(4), 2391–2403 (1999)
15. Chamoin, L., Oden, J.T., Prudhomme, S.: A stochastic coupling method for atomic-to-continuum Monte Carlo simulations. Comput. Methods Appl. Mech. Engng. **197**, 3530–3546 (2008)
16. Chamoin, L., Prudhomme, S., Ben Dhia, H., Oden, J.T.: Ghost forces and spurious effects in atomic-to-continuum coupling methods by the Arlequin approach. Int. J. Numer. Meth. Engng. **83**(8-9), 1081–1113 (2010)
17. Curtin, W., Miller, R.: Atomistic/continuum coupling in computational material science. Modeling and Simulation in Materials Science and Engineering **11**, R33–R68 (2003)
18. Dobson, M., Luskin, M.: Analysis of a force-based quasicontinuum approximation. Mathematical Modelling and Numerical Analysis **42**(1), 113–139 (2009)
19. Dobson, M., Luskin, M.: An optimal order error analysis of the one-dimensional quasicontinuum approximation. SIAM Journal on Numerical Analysis **47**(4), 2455–2475 (2009)
20. E, W., Engquist, B., Huang, Z.: Heterogeneous multiscale method: A general methodology for multiscale modeling. Physical Review B **67**, 092,101 (2003)
21. E, W., Engquist, B., Li, X., Ren, W., Vanden-Eijnden, E.: Heterogeneous multiscale methods: A review. Communications in Computational Physics **2**(3), 367–450 (2007)
22. Fish, J.: Bridging the scales in nano engineering and science. Journal of Nanoparticle Research **8**(6), 577–594 (2006)
23. Fish, J.: Multiscale Methods: Bridging the Scales in Science and Engineering. Oxford University Press (2009)
24. Fish, J., Nuggehally, M., Shephard, M., Picu, C., Badia, S., Parks, M., Gunzburger, M.: Concurrent atc coupling based on a blend of the continuum stress and the atomic force. Computer Methods in Applied Mechanics and Engineering **196**, 4548–4560 (2007)

25. Miller, R.E., Tadmor, E.B.: The quasicontinuum method: overview, applications and current directions. Journal of Computer-Aided Materials Design **9**, 203–239 (2002)
26. Prudhomme, S., Ben Dhia, H., Bauman, P.T., Elkhodja, N., Oden, J.T.: Computational analysis of modeling error for the coupling of particle and continuum models by the Arlequin method. Computer Methods in Applied Mechanics and Engineering **197**, 3399–3409 (2008)
27. Prudhomme, S., Chamoin, L., Ben Dhia, H., Bauman, P.T.: An adaptive strategy for the control of modeling error in two-dimensional atomic-to-continuum coupling simulations. Computer Methods in Applied Mechanics and Engineering **198**, 1887–1901 (2009)
28. Tadmor, E.B., Ortiz, M., Phillips, R.: Quasicontinuum analysis of defects in solids. Philosophical Magazine **A73**, 1529–1563 (1996)
29. Wagner, G.J., Liu, W.K.: Coupling of atomistic and continuum simulations using a bridging scale decomposition. Journal of Computational Physics **190**, 249–274 (2003)
30. Xiao, S.P., T. Belytschko, T.: A bridging domain method for coupling continua with molecular dynamics. Computer Methods in Applied Mechanics and Engineering **193**, 1645–1669 (2004)